Motion of Spin Label Side Chains in Cellular Retinol-Binding Protein: Correlation with Structure and Nearest-Neighbor Interactions in an Antiparallel β-Sheet†

Michael A. Lietzow‡ and Wayne L. Hubbell*

Jules Stein Eye Institute and Department of Chemistry and Biochemistry, University of California, Los Angeles, California 90095-7008

Received November 21, 2003; Revised Manuscript Received January 26, 2004

ABSTRACT: A goal in the development of site-directed spin labeling in proteins is to correlate the motion of a nitroxide side chain with local structure, interactions, and dynamics. Significant progress toward this goal has been made using α-helical proteins of known structure, and the present study is the first step in a similar exploration of a β-sheet protein, cellular retinol-binding protein (CRBP). Nitroxide side chains were introduced along both interior and edge strands. At sites in interior strands, the side-chain motion is strongly influenced by interactions with side chains of neighboring strands, giving rise to a rich variety of dynamic modes (weakly ordered, strongly ordered, immobilized) and complex electron paramagnetic resonance spectra that are modulated by strand twist. The interactions giving rise to the dynamic modes are explored using mutagenesis, and the results demonstrate the particular importance of the non-hydrogen-bonded neighbor residue in giving rise to highly ordered states. Along edge strands of the β-sheet, the motion of the side chain is simple and weakly ordered, resembling that at solvent-exposed surfaces of an α-helix. A simple working model is proposed that can account for the wide variety of dynamic modes encountered. Collectively, the results suggest that the nitroxide side chain is an effective probe of side-chain interactions, and that site-directed spin labeling should be a powerful means of monitoring conformational changes that involve changes in β-sheet topology.

One of the goals in developing SDSL[1] methodology is to interpret the motion of individual nitroxide side chains in terms of local protein structure and dynamics. Using mutagenesis (*1*, *2*), X-ray crystallography (*3*), and quantitative analysis of the EPR spectra of spin-labeled proteins (*4*, *5*), progress has been made toward this goal for α-helical proteins (*6*, *7*). For example, both X-ray and spectroscopic evidence supports the motional model shown in Figure 1 for the most commonly used nitroxide side chain (designated R1) at solvent-exposed α-helical sites. In this model, the S_δ of the disulfide bond interacts with main-chain atoms, thereby constraining rotations about dihedrals χ_1 and χ_2. Because isomerization of the disulfide (χ_3) is slow on the EPR time scale, limited torsional oscillations about χ_4 and χ_5 probably dominate the motion of the nitroxide ring (Figure 1B) and give rise to the experimentally observed EPR spectra that are characteristic of an ordered state (Figure 1C) (*4*). Because the anisotropic magnetic interactions of the nitroxide are not completely averaged by the ordered internal motion of the side chain, the EPR spectra are sensitive to any additional

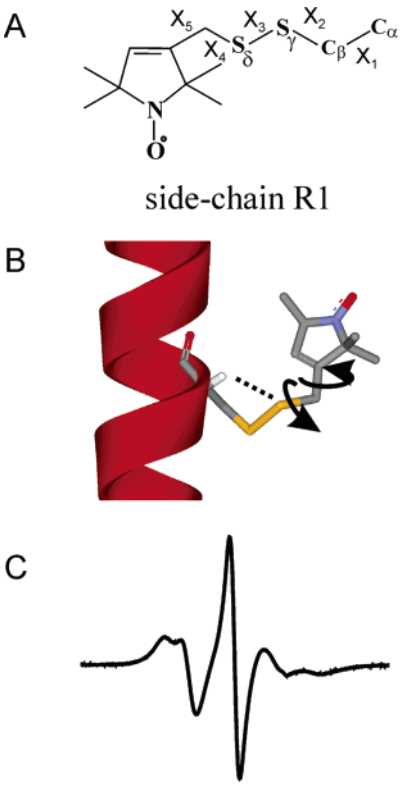

FIGURE 1: R1 side-chain structure, showing definition of the dihedral angles (A), the conformation and motion of the side chain at solvent-exposed sites on α-helices (B), and the EPR spectrum of T4L 72R1 (C). The dashed line in (B) identifies an apparent interaction of the S_δ atom with the $C_\alpha H$ hydrogen atom.

† This work was supported by NIH Grants EY05216 and T32 EY07026, the Jules Stein Professor Endowment, and a grant from the Ford Bundy and Anne Smith Bundy Foundation.

* To whom correspondence should be addressed. E-mail: hubbellw@jsei.ucla.edu. Telephone: (310) 206-8830. Fax: (310)794-2144.

‡ Present address: The Scripps Research Institute, 10550 Torrey Pines Rd., MB-2, La Jolla, CA 92037.

[1] Abbreviations: SDSL, site-directed spin labeling; EPR, electron paramagnetic resonance; CRBP, cellular retinol-bining protein; WT, wild-type CRBP; NiEDDA, nickel(II) ethylenediaminediacetate; MOMD, microscopic order/macroscopic disorder; T4L, T4 lysozyme; HB, hydrogen-bonded; NHB, non-hydrogen-bonded.

10.1021/bi0360962 CCC: $27.50
Published on Web 02/25/2004

motions in the gigahertz regime that might be present. For example, site-dependent variations in the rate and order of R1 motion have been analyzed in terms of protein backbone fluctuations (*5*).

If the nitroxide moiety of R1 in α-helices interacts with other groups in the environment, the simple internal motion described above is modulated and new dynamic modes arise. By correlating particular interactions with the dynamic modes, the EPR spectra can be used to provide detailed information on the local environment. For example, a highly ordered state of R1 appears to be correlated with a C−H··· ·O hydrogen bond between the nitroxide ring and tyrosine, while other strongly immobilized but solvent-accessible states arise from hydrophobic tertiary interactions of the nitroxide ring (*3*). In cases where the nitroxide interaction is of tertiary origin, the dynamic state of the side chain is a sensitive indicator of conformational changes (*8*).

The above studies establish SDSL as a useful tool for the determination of structure, for the detection of conformational changes, and for the determination of backbone fluctuations in α-helical structures. Although spin-labeling studies of *β*-sheet proteins have been reported (*9*, *10*), the present study is the first to report a systematic exploration of R1 side-chain dynamics in a *β*-protein of known structure. For this study, cellular retinol-binding protein (CRBP) was selected. CRBP is a member of the intracellular lipid-binding protein family and is responsible for the transport of *all-trans*-retinol from the plasma membrane to various intracellular targets. The crystal structure of *holo*-CRBP is known to 2.1 Å resolution (*11*), and NMR structures have been determined for the solution state in both the apo and holo forms (*12*). The molecule consists of 10 antiparallel strands organized into two orthogonal sheets that form a flattened barrel. A cavity between the sheets forms the retinol-binding site.

The structural constraints on side-chain motions in *β*-sheets are fundamentally different from those in α-helices. For example, nearest-neighbor side chains in α-helices ($i \pm 3$, $i \pm 4$) show little interaction with R1 at most solvent-exposed sites (*1*) due to the large spacing of the side chains and the fact that they project radially outward, away from each other. On the other hand, nearest-neighbor side chains in a flat *β*-sheet are more closely spaced than in the α-helix and lie essentially parallel to one another. Thus, significant side chain−side chain interactions are expected, consistent with the context-dependent propensities for *β*-sheets (*13*−*17*). The results reported here, based on mutagenesis of neighboring side chains, clearly reveal the effect of direct interactions of R1 in interior strands with nearest-neighbor side chains in flanking strands. The strength and nature of the interaction depend on three factors, namely the identity of the neighboring residue, whether that residue is located at the hydrogen-bonded or non-hydrogen-bonded neighbor site, and the degree of strand twisting. These features give rise to a variety of dynamic modes of the nitroxide side chain. On the other hand, R1 residues in edge strands have a simple motion similar to R1 on solvent-exposed surfaces of helices. The wide variety of complex EPR spectra arising from R1 in *β*-sheets can be understood in terms of a simple working model wherein the R1 side chain is a direct probe of side chain−side chain interactions, and the EPR spectra are expected to provide information on strand registration and on conformational changes that affect the degree of twist.

MATERIALS AND METHODS

Preparation of Mutants, Protein Purification, and Spin Labeling. The rat cellular retinol-binding protein gene in a pT7-7 plasmid vector was kindly provided by Dr. David. E. Ong (Vanderbilt University). Site-directed mutagenesis was performed using the overlap extension PCR method as described by Ho et al. (*18*). The coding and flanking region was excised at *Cla*I and *Nde*I restriction sites and inserted into the pT7-7 cloning vector using T4 ligase. First, a cysteine-less "pseudo wild-type" gene was prepared by replacing the three native cysteines (82, 95, and 126) with alanines. This construct was used as the template for all single-substitution mutations, and protein expressed from this construct will be referred to below as WT or CRBP. To ensure fidelity of Taq polymerase, the entire coding region for each mutant construct was sequenced using ABI Prism Dye Deoxy Terminator Cycle Sequencing. Double mutations were constructed as above using the appropriate mutant construct as a template.

Competent *Escherichia coli* BL21 DE3 pLysS cells were transformed with mutant plasmids. Cells were grown to mid log-phase at 37 °C in LB media containing 0.5% (w/v) casamino acids and 100 μg/mL ampicillin. At $OD_{600} \approx 0.6$, the temperature was decreased to 29 °C, and protein expression was induced by the addition of isopropyl *β*-thiogalactoside to a final concentration of 0.5 mM. Cells were harvested by centrifugation 3 h after induction, resuspended in 10 mM Tris (pH 7.6), 100 mM KCl, 1 mM EDTA, and 5 mM dithiothreitol, and lysed by sonication. This solution was treated with 10% polyethyleneimine to a final concentration of 0.2% and centrifuged to remove precipitated nucleic acids. The supernatant was further treated by ammonium sulfate fractionation at 50% and 80%, with the 80% pellets containing the bulk of the CRBP. The 80% pellets were resuspended in 20 mM Tris/acetate (pH 8.3) and 5 mM dithiothreitol and applied to a Superdex 75 gel filtration column (Pharmacia) at a flow rate of 1 mL/min. Fractions were collected and screened for CRBP, which eluted as a broad peak. Fractions containing CRBP were pooled and concentrated to approximately 5 mL using an Amicon YM-10 filter. This solution was loaded as ≤1 mL aliquots on a Superdex 75 column (Pharmacia) equilibrated with 20 mM sodium phosphate (pH 7.0) and 100 mM NaCl. Fractions were collected and screened by Coomassie-stained SDS−PAGE for CRBP. Fractions that were homogeneous for CRBP were either frozen or used immediately for the nitroxide-labeling reaction described below.

A portion of the CRBP-containing fraction from the Superdex 75 column was incubated with a 10-fold molar excess of (1-oxyl-2,2,5,5 tetramethylpyrroline-3-methyl) methanethiosulfonate (*19*) or the diamagnetic analogue (1-acetyl-2,2,5,5 tetramethylpyrroline-3-methyl) methanethiosulfonate (*20*, *21*) (both gifts of Kálmán Hideg, University of Péc, Hungary) and allowed to react for 4−12 h at room temperature, with the longer reaction times being allotted for buried sites. Unreacted label was removed by gel filtration on a G25 Sephadex fast-desalting HPLC column (Pharmacia) equilibrated with 20 mM sodium phosphate (pH 7.0) and 100 mM NaCl. At this point, CRBP is in the apo form. To produce *holo*-CRBP, *all-trans*-retinol was added in excess from an ethanol stock solution such that the final ethanol

concentration did not exceed 1% of the sample volume. The solubility of retinol is extremely low, and essentially all excess precipitated and was removed by centrifugation. The supernatant was concentrated, and quantitative binding of retinol was confirmed by the UV−vis absorption spectrum of the protein, which showed a ratio of absorbance $A_{348}/A_{280} \approx 1.4$, similar to that reported for recombinant CRBP (*22*).

EPR Spectroscopy and Fitting of EPR Spectra. Approximately 5 μL of spin-labeled proteins (typically 50−300 μM) in 20 mM phosphate buffer (pH 7), 100 mM NaCl, and 30% (w/v) sucrose was loaded into Pyrex capillaries (0.84 o.d. × 0.64 i.d.; VitroCom Inc., Mountain Lakes, NJ), and spectra were recorded at 23 ± 1 °C using a Varian E-109 spectrometer fitted with a loop-gap resonator (*23*). The incident microwave power was 2 mW, and the 100 kHz modulation amplitude was optimized for maximum signal without distortion of the line shape.

Measurements of the accessibility parameters for O_2 and NiEDDA were carried out in TPX capillaries by the power saturation method previously described (*24*). The O_2 concentration was that in equilibrium with air, and the NiEDDA concentration was 5 mM.

EPR spectra were fit in a least-squares sense to the MOMD model of Freed and co-workers using the program NLSL described by Budil et al. (*25*). For all simulations, the principal values of the **A** and **g** tensors were fixed at $A_{xx} = A_{yy} = 6$ G, $A_{zz} = 37$ G, $g_{xx} = 2.0076$, $g_{yy} = 2.0050$, and $g_{zz} = 2.0023$. These values are appropriate for the nitroxide of R1 on solvent-exposed surfaces in proteins (*4*). Spectra were simulated using an axially symmetric diffusion tensor, with principal values R_{par} and R_{perp}. In this report, spectra are characterized by the geometric mean of the diffusion tensor elements, $\bar{R} = (R_{par}R_{perp}^2)^{1/3}$, and an asymmetry parameter, $N = R_{par}/R_{perp}$ (*25*). The mean correlation time, τ, is defined as $\tau = 1/6\bar{R}$. In the MOMD model, diffusion of the nitroxide is constrained by an ordering potential U, which is expanded in a series of spherical harmonics,

$$U(\Omega) = -k_B T \sum_{L,K} c_K^L D_{0K}^L(\Omega)$$

where $\Omega = (\alpha,\beta,\gamma)$ are the angles relating the diffusion frame to a frame fixed on the protein (the "director" frame). For the fits in this report, only the first term in the expansion, with coefficient C_0^2, is required for a reasonable fit. The order parameter, S_{20}, is calculated from C_0^2 as described by Schneider and Freed (*26*).

The diffusion tensor is related to the molecular frame of the nitroxide by a transformation involving the three Euler angles α_D, β_D, and γ_D (the diffusion tilt angles). For approximately axially symmetric nitroxide magnetic and diffusion tensors, only β_D, the polar angle between the z-axis of the diffusion tensor and that of the nitroxide molecular frame, is important. For solvent-exposed R1 side chains, where an ordered motion is due to constraints on the disulfide bond of the nitroxide, it was previously found that $\beta_D \approx 36°$ accounts well for spectra, and that value is fixed in the fits to reduce the number of parameters (*4*).

Thus, for a single population, the parameters $\bar{R}$, N, C_0^2, and the Lorentzian homogeneous (w) and Gaussian inhomogeneous line widths (gib0, gib2) were varied for the best fit. For the R1 side chain, the motion of the ring is due to torsional oscillations about the bonds that connect it to the backbone. For dynamic modes where the nitroxide ring does not interact directly with the protein, the torsional oscillation rates about the various bonds are assumed to be similar, and $R_{par} \approx R_{perp}$. Thus, fitting is begun with $N = 1$, and significant deviations are explored only in the case that satisfactory fits could not be obtained. Generally, it is found that the best fits are obtained with N in the range of 1−1.3. As is well known, the fitting parameters $\bar{R}$ and C_0^2 can be correlated and are not accurately determined from a fit to a single EPR frequency (*25*). Thus, the rates and orders determined from fits to a single frequency are to be viewed as estimates. However, rate and order correlation can often be at least partially resolved because, for the common dynamic modes of the R1 side chain, rates have a strong effect on the spectral line widths, while ordering has a comparatively small effect (L. Columbus and W. L. Hubbell, unpublished results). Thus, fitting is begun with Lorentzian and Gaussian line width parameters set to 0, and rate parameters are varied to get approximate fits to the center line width. In most cases, variations in either rate or order can be compensated by the other only within a range of about ±20%.

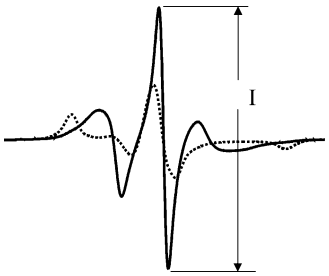

FIGURE 2: EPR spectra of 75R1 in *holo*- (solid trace) and *apo*- (dashed trace) CRBP.

EPR Assay for Determination of Retinol Binding Affinity to CRBP. An exchange assay was developed to measure the *all-trans*-retinol binding affinity of each spin-labeled mutant relative to that of the WT protein. In a separate study (results to be published elsewhere), a large difference in the EPR spectra of the apo and holo forms of the spin-labeled mutant CRBP 75R1 was discovered (Figure 2). The assay used here exploits this difference to determine the fraction, f_{holo}, of the holo form in a mixture. The intensity of the central resonance line (I) of the composite spectrum provides a simple empirical parameter that changes linearly with f_{holo}. To calibrate I as a measure of f_{holo}, mixtures of *apo*- and *holo*-75R1 were prepared that contained the same total amount of protein (300 μM), with f_{holo} varying from 0 to 1. Values of f_{holo} were plotted as a function of I/I_o, where I_o is the intensity of the pure *holo*-75R1 sample. The plot was well fit by the linear equation $f_{holo} = 1.248(I/I_o) - 0.237$ ($r^2 = 0.995$), which was then used to determine f_{holo} from measured intensities in mixtures of *apo*- and *holo*-75R1.

When *holo*-75R1 is mixed with *apo*-CRBP, or a mutant thereof, retinol is rapidly exchanged, and the value of f_{holo} at equilibrium is a direct measure of the relative binding affinity of 75R1 and the other (acceptor) protein. Measurement of f_{holo} by the method described above is complicated if the acceptor protein is also spin-labeled. To circumvent this problem, cysteine mutants of interest were labeled with a diamagnetic analogue of R1, designated R1′, that is essentially isomorphous with R1 but has no EPR signal (*20*,

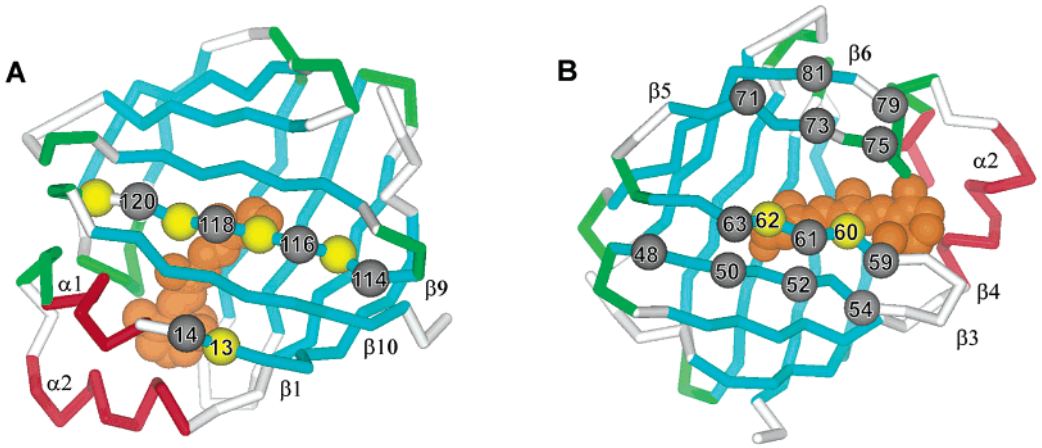

FIGURE 3: Ribbon models of CRBP (*11*) showing labeling sites (as spheres at the α-carbons) in center strand β3 (48, 50, 52, 54), center strand β9 (114, 115*, 116, 117*, 118, 119*, 120, 121*), edge strand β1 (13, 14), edge strand β4 (59, 60*, 61, 62*, 63), edge strand β5 (71, 73), and edge strand β6 (81). Sites marked with asterisks and colored yellow in the figure are buried, and the side chains project into the retinol-binding cavity. Site 75 is in the β5−β6 turn, and 75R1 is used in the exchange assay for retinol binding (see Methods). Retinol is shown as an orange CPK model.

21). With this strategy, the relative dissociation constant of any CRBP mutant labeled with R1′ can be calculated from experimentally determined values of f_{holo} as described below.

Let the dissociation constants of retinol from *holo*-75R1, *holo*-CRBP, and *holo*-XR1′, where XR1′ is a mutant of CRBP with R1′ at site X, be K_{D1}, K_{D2}, and K_{D3}, respectively. In an equilibrium mixture formed from equimolar amounts of *holo*-75R1 and *apo*-CRBP,

$$K_{D1}/K_{D2} = \{[\textit{apo}\text{-75R1}]/[\textit{holo}\text{-75R1}]\}_{1,2}^{\ 2} = [1/f_{holo} - 1]_{1,2}^{\ 2} \equiv (R_{1,2})^2 \quad (1)$$

Likewise, in an equilibrium mixture formed from equimolar amounts of *holo*-75R1 and *apo*-XR1′,

$$K_{D1}/K_{D3} = \{[\textit{apo}\text{-75R1}]/[\textit{holo}\text{-75R1}]\}_{1,3}^{\ 2} = [1/f_{holo} - 1]_{1,3}^{\ 2} \equiv (R_{1,3})^2 \quad (2)$$

Combining (*1*) and (*2*),

$$(K_{D1}/K_{D2})/(K_{D1}/K_{D3}) = K_{D3}/K_{D2} = (R_{1,2})^2/(R_{1,3})^2 \quad (3)$$

Finally, the free energy change for ligand dissociation, relative to CRBP, is given by

$$\Delta G_{D,XR1'} - \Delta G_{D,CRBP} = \Delta\Delta G_D = -RT \ln K_{D3}/K_{D2} = -RT \ln\{(R_{1,2})^2/(R_{1,3})^2\} \quad (4)$$

Exchange measurements were made by preparing solutions containing 300 μM *holo*-75R1 and 300 μM of either *apo*-CRBP or the apo form of mutant containing R1′ at the desired position in 20 mM sodium phosphate (pH 7.0) and 100 mM NaCl.

Modeling of the R1 Side Chain in CRBP. Modeling of CRBP (Protein Data Bank code 1CRB) was done in either DS Viewer Pro or InsightII (Accelerys, San Diego). The R1 side chain was built at the desired site, and the structure was optimized by variation in the structure of R1 only; generally, the native side chains were left in their native configurations, and in a few cases slight changes made in the dihedral angles (only beyond χ_1) of nearby residues. Allowed rotamers were determined by manual changes in dihedrals of R1, using the bump monitor to eliminate states with overlap. Values of χ_1, χ_2 were fixed at 60 ± 10°, −60 ± 10°, or 180 ± 10°. Values of χ_3 (the S−S dihedral) were limited to ±90 ± 10°.

RESULTS

Figure 3 shows the sites in CRBP where R1 side chains were introduced, one at a time, in the present study. In each case, the cysteine substitution mutants expressed in high yield and reacted essentially quantitatively with the spin label reagent. These particular residues were selected to represent sites in interior strands, i.e., sites flanked on either side by H-bonded adjacent strands, and in edge strands, where only one side is flanked by another H-bonded strand. Residues 48−54 and 114−120 are located in interior strands β3 and β9, respectively. Residues in edge strands include 13 and 14 in β1, 59−63 in β4, 71−73 in β5, and 81 in β6. Residue 75, in the β5−β6 interstrand turn, is used in the exchange assay for retinol binding affinity described in Methods.

The primary focuses of this study are the solvent-accessible residues on the outer surface of the β-sheets, although a few buried sites are included for completeness (yellow spheres in Figure 3). All of the mutants bearing a spin label at solvent-accessible sites bound retinol to form a *holo*-protein, and the dissociation constants and corresponding free energies, relative to CRBP, are given in Table 1.

About half of the mutants decrease $\Delta\Delta G_D$ (increase the dissociation constant, K_D), and half increase it, although the effects are small, except at R120R1′. To put the values in context, the free energy of retinol dissociation for CRBP has been reported to be in the neighborhood of 10 kcal/mol (*22*). The largest perturbation in free energy due to the spin label is for R120R1′, where $\Delta\Delta G_D$ is about 30% of this value. The relative dissociation free energies for the remaining mutants are within 10% of the estimated value for CRBP, with most being within 5%. Thus, the presence of the spin label at solvent-exposed sites has relatively little effect on the ligand affinity. On the other hand, the spin label at buried sites, where the side chain projects directly into the binding cavity, seriously perturbs ligand binding, as expected (data not shown).

Table 1: Relative Dissociation Constants and Free Energies for CRBP Mutants

class	mutant	$K_D/K_{D,WT}$	$\Delta\Delta G_d$ (kcal/mol)
edge strand	E41R1′	0.87	0.083
	N59R1′	1.8	−0.34
	I61R1′	1.5	−0.22
	D63R1′	5.0	−0.95
	E71R1′	0.86	0.086
	D73R1′	1.2	−0.12
	K81R1′	0.93	0.041
interior strand	H48R1′	0.68	0.22
	I50R1′	1.1	−0.073
	R52R1′	1.4	−0.19
	L54R1′	0.35	0.62
	E114R1′	0.71	0.20
	E116R1′	6.4	−1.1
	E118R1′	0.81	0.12
	R120R1′	130	−2.9

In the following studies, the spin-labeled derivatives of CRBP at solvent-accessible sites were studied in the holo form only. On the basis of the data of Table 1 and the estimated dissociation constant for CRBP, the dissociation constant for the various spin-labeled proteins lies in the range of 10−60 nM, except for 120R1, which is 100-fold greater. The concentration of protein in the EPR experiments is near 300 μM. Therefore, in most cases, only ~1% of the protein is dissociated at equilibrium with the apo form. Thus, in all but 120R1, the EPR spectra correspond to essentially the pure holo form of the labeled proteins. For 120R1, the amount of apo form is still less than ~10%.

R1 Motion at Solvent-Exposed Sites in Interior Strands β3 and β9 of holo-CRBP (*48*, *50*, *52*, *54*; *114*, *116*, *118*, *120*). β-Sheets and individual strands are characterized in part by twist and pleat. As the degree of twist increases, neighboring side chains point away from each other, reducing side-chain interactions. The degree of twist of the strands considered here can be seen in the plot of Figure 4A for residues in β3 (48−54, red dots) and β9 (114−121, blue dots). Residues 49−53 in β3 lie near the $n = 2$ line of the Ramachandran plot in Figure 4A, indicating little twist through this sequence, and the sheet formed from β2−β4 is essentially flat. The N- and C-terminal residues in β3, 48 and 54, respectively, have positive twists that match them to the adjacent turns. Residues in β9 lie above the $n = 2$ line, indicating a right-handed twist in the β8−β10 sheet. These features can be appreciated from Figure 4B,C, which shows side views of the two sheets.

Figure 5 presents the EPR spectra of R1 at solvent-exposed sites in interior strands β3 and β9. The off-set dotted traces are the fits of the spectra to the MOMD model, as described above. The relevant parameters of the fits are given in Table 2, and these will be discussed below with respect to each site.

A notable feature of the R1 spectra is the wide range of R1 dynamic modes, as reflected in the EPR spectral line shapes. At one extreme is 118R1, where the nitroxide has relatively high mobility. The spectrum of 118R1 can be fit with rotary diffusion rates corresponding to a mean correlation time of $\tau \approx 2.3$ ns and a weak orientation potential corresponding to an order parameter of $S_{20} \approx 0.2$. It is of interest to compare this motion to that for R1 on a solvent-exposed helix surface site (Figure 1C). Site 72R1 in T4 lysozyme (T4L) has been studied in detail, and the motion of the side chain was found to be determined primarily by internal modes in the side chain (*4*). That is, the motion of the nitroxide is due primarily to torsional oscillations about the bonds in the side chain, with little modulation from interactions of the side chain or from backbone motions. For T4L 72R1, the spectrum can be accurately fit to the MOMD model with $\tau \approx 2$ ns and $S_{20} \approx 0.47$. Thus, for CRBP 118R1, the rate is about the same, but the order of motion is significantly reduced relative to the same side chain on a rigid helix surface site.

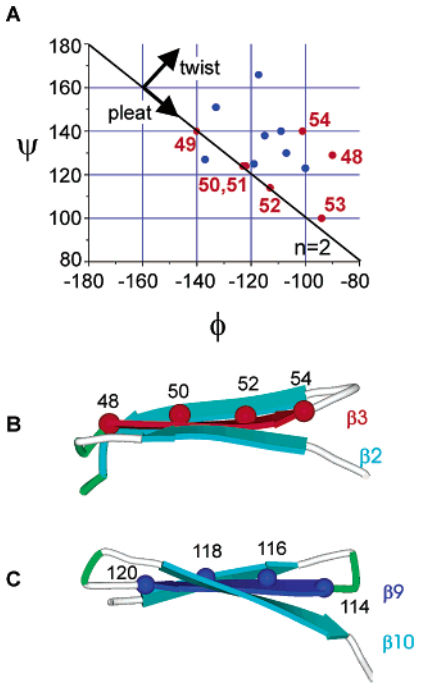

FIGURE 4: Geometry of the strands and sheets constituting the regions investigated. (A) A Ramachandran plot of residues in β3 and β9. (B) Side view of β3 and flanking strands. (C) Side view of β9 and flanking strands.

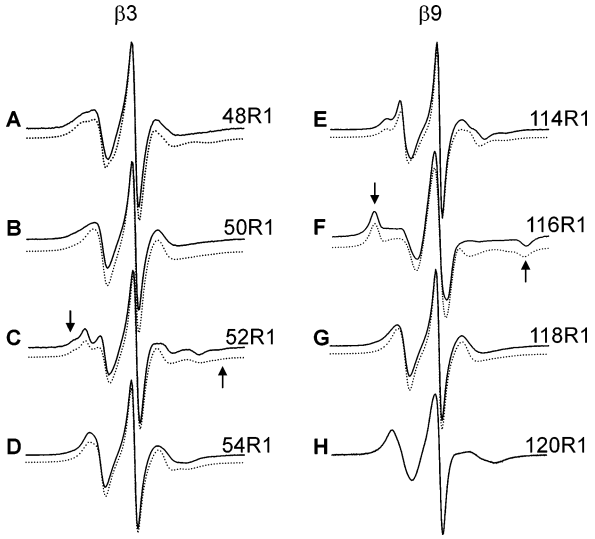

FIGURE 5: EPR spectra for R1 at solvent-exposed sites in center strands of *holo*-CRBP. Arrows in (C) and (F) mark the hyperfine extrema corresponding to immobilized states of the nitroxide. The scan width is 100 G. The solid traces are experimental spectra, and the dotted traces are the least-squares best fits to the MOMD model (see Methods).

Table 2: Parameters for Fits to the Spectra

residue	τ (ns)	N	S_{20}	occupancy (%)
118R1	2.3	1	0.2	100
116R1 comp 1	4.6	1	0.13	56
116R1 comp 2 (immobile)	~20			44
114R1 comp 1	1.7	1.3	0	48
114R1 comp 2	2.1	1.3	0.58	52
48R1 comp 1	1.6	1.3	0.17	20
48R1 comp 2	5.3	1.3	0.16	80
50R1 comp 1	2.2	1	0.27	90
50R1 comp 2	8	1	0	10
52R1 comp 1	1.3	1.3	0.7	88
52R1 comp 2 (immobile)	17	1	0	12
54R1	2.4	0.7	0.35	100
E41Q/52R1	1.1	1.0	0.55	100
E41K/52R1	1.3	1.3	0.55	100
E41T/52R1	1.7	1.3	0.56	100
E41D/52R1 comp 1	1.7	1.3	0.57	61
E41D/52R1 comp 2	17			39
52R1/I61L	1.7	1.3	0.5	100
52R1/I61V comp 1	1.3	1.3	0.71	57
52R1/I61V comp 2	17			43
52R1/I61T comp 1	1.2	1.3	0.56	65
52R1/I61T comp 2	12			34
52R1/I61E comp 1	3	1.3	0	40
52R1/I61E comp 2	12	1.3	0	60
14R1	2.2	0.13	0.3	100
59R1	2.6	1	0.48	100
61R1	2	1	0.48	100
63R1	1.9	1	0.47	100
71R1	1.9	1	0.47	100
73R1	2.2	0.5	0.3	100
W109L/116R1 comp 1	2.1	1.3	0.5	90
W109L/116R1 comp 2	20	1	0	10
81R1 comp1	3.7	1	0.33	70
81R1 comp2	5	0.1	0.57	30

At the other extreme in R1 mobility is 116R1, also in β9. The spectrum of 116R1 requires two dynamic components for a reasonable fit, one that is strongly immobilized and recognized by the well-resolved hyperfine extrema (arrows in Figure 5). The immobilized component, corresponding to 44% of the population, is fit by an isotropic motion with $\tau \approx 20$ ns. Because an immobile spectral component at a surface site could arise from concentration-dependent oligomerization, serial dilutions were made for each surface site mutant exhibiting an immobile component. Unless noted otherwise, the EPR spectra for all mutants reported were concentration-independent, indicating the absence of effects due to oligomerization. The second component of 116R1 is characterized by $\tau \approx 4.6$ ns and a weak ordering with $S_{20} \approx 0.13$. In the 30% sucrose solutions used in the present experiments, the rotational correlation time of CRBP, assuming Stokes−Einstein behavior, is $\tau \approx 18$ ns. Thus, one state of R1 at site 116 is essentially immobilized with respect to the protein.

The highly mobile 118R1 and the immobilized component of 116R1 represent the extreme cases of dynamic modes of R1 along the center strand sites. Other sites are of relatively high mobility, similar to 118R1 (50R1, 54R1), or have multiple components (48R1, 52R1, 114R1). The spectrum of 52R1 is particularly striking due to the presence of three resolved hyperfine extrema, one set of which corresponds to a relatively immobilized state (marked by arrows in Figure 5). This spectrum can be reasonably well simulated by two dynamic populations, one with isotropic motion ($\tau \approx 16.7$ ns, 12%) and the other having rapid, anisotropic motion with high order ($\tau \approx 1.3$ ns, $S_{20} \approx 0.7$, 88%). Models to account for this high degree of order will be discussed below.

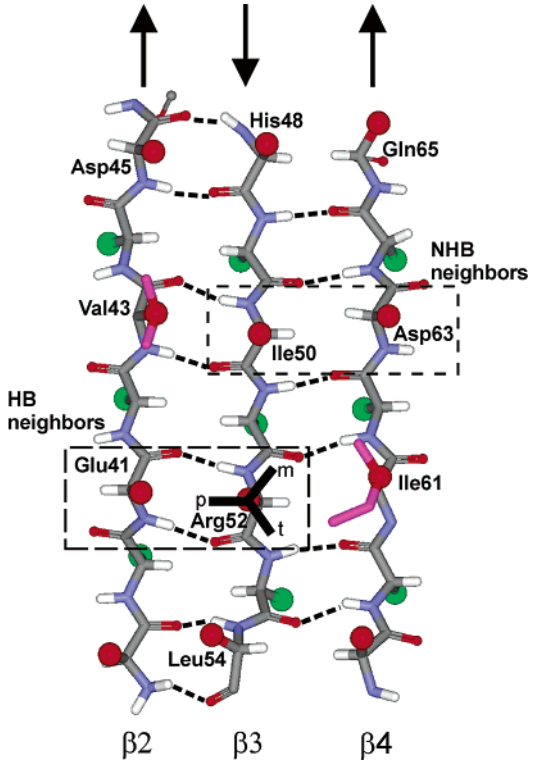

FIGURE 6: Structure of the CRBP β-sheet around site 52. The H-bonded and non-H-bonded neighbors in adjacent strands are identified by the dashed boxes. The solid black lines on residue 52 indicate the direction of the β-carbon atom in rotamers about the $C_\beta-C_\gamma$ dihedral (χ_1). The rotamer designation of Lovell et al. (*28*) is used. In this convention, the χ_1 dihedral is measured from the backbone N atom. The three rotamers, representing the low-energy staggered configurations, are designated as m, p, or t, corresponding to a χ_1 of −60° (minus), +60° (plus), or 180° (trans), respectively.

What features of the structure are responsible for these variations in side-chain dynamics from site to site? NMR ^{15}NH relaxation studies of *holo*-CRBP in solution indicate that the backbone motions along strands β3 and β9 are relatively constant and equal in the two strands, with N−H bond vector order parameters of $0.91 \leq S_{NH} \leq 0.95$ (*12*). Therefore, the wide variation of R1 side-chain dynamics does not likely originate entirely from site-dependent backbone dynamics, but must arise from direct interactions of R1 with either main-chain atoms or neighboring side chains.

The aim of the present investigation is to identify the likely molecular origins of these interactions, and the experimental strategy is a systematic variation of the neighboring side chains and analysis of the concomitant change in side-chain dynamics. For this purpose, sites 52R1, 54R1, and 116R1 have been selected for investigation. These sites were selected because the EPR spectra of 52R1 and 116R1 reveal multiple components, one of which corresponds to a relatively immobilized state of the side chain that must arise from side-chain interactions. Moreover, 52 and 116 reside in sheets with significantly different degrees of twist (Figure 4), providing an opportunity to examine the effect of this feature. 54R1 is of interest because its spectrum is characteristic of an anisotropic motion similar to that for R1 on helix surface sites.

Interactions of 52R1. Figure 6 shows a section of the β2−β4 sheet from CRBP and identifies the key features of the antiparallel β-sheet relevant to side-chain interactions. For

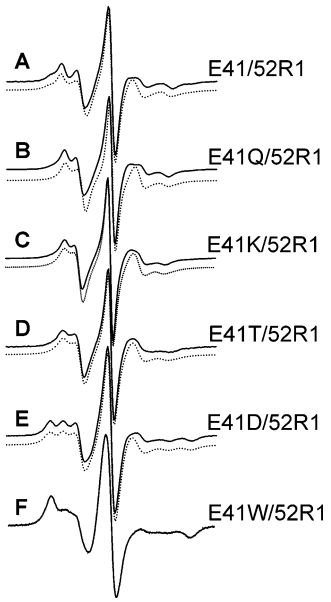

FIGURE 7: EPR spectra of CRBP 52R1 with various side chains substituted for HB neighbor E41. The solid traces are experimental spectra, and the dotted traces are the least-squares best fits to the MOMD model (see Methods).

a residue in an interior strand of a β-sheet, the neighboring side chains in closest proximity are those on adjacent strands. For example, residues 41 and 61 are the nearest neighbors to 52. There are two categories of such nearest neighbors, one of which is directly H-bonded to the residue in question (HB neighbor) and the other of which is not (NHB). For residue 52, E41 and I61 are the HB and NHB neighbors, respectively. The $C_\alpha-C_\alpha$ distance between HB neighbors is typically 5.5 Å, while that for NHB neighbors is 4.5 Å. For β-branched side chains, the bulky branch points inward toward the NHB neighbor and away from the HB neighbor, as illustrated by I61 and V43 in Figure 6. Thus, a β-branched residue at the NHB site is expected to give rise to side-chain interactions. Finally, the orientation of the $C_\beta-C_\gamma$ bond in the 52 side chain is indicated for the three χ_1 rotamers (p, m, and t) for native side chains in β-sheets (see legend of Figure 6 for definitions).

To identify the interaction responsible for the immobilized component in the spectrum of 52R1, and to identify the origin of the unusually high order of the second component, neighboring residues were mutated. In a β-strand, the *intra*strand neighbors on the same surface are typically 6.5−7 Å away ($C_\alpha-C_\alpha$), depending on the degree of pleating, compared to 4.5−5.5 Å for the NHB and HB *inter*strand neighbors. Thus, significant intrastrand interactions are not anticipated. To test this expectation, intrastrand residue I50 was mutated to either valine or leucine. These mutations produced no change in the spectrum of 52R1, suggesting no interaction between residue 50 and 52R1 (data not shown). On the other hand, mutations at either 41 or 61 produced dramatic changes in the spectrum of 52R1.

Mutations of the H-Bonding Neighbor, E41. First, consider mutations at the HB residue E41. Figure 7 shows the EPR spectra for the various mutations at E41. The offset dotted traces are again the simulated spectra. Figure 7A shows the spectrum of the 52R1 with the native neighbors for reference. Figure 7B shows the spectrum of 52R1 in the mutant E41Q. As is evident, the most immobilized component has essentially disappeared, and the spectrum is reasonably well fit to a single component that strongly resembles that of the ordered component in the spectrum of 52R1 with native neighbors ($\tau \approx 1.1$ ns, $S_{20} \approx 0.55$). Similar results are obtained when E41 is substituted with lysine (Figure 6C) or the β-branched residue threonine (Figure 6D). In each case, the spectrum can be represented by a single component with best-fit parameters similar to those of the E41Q mutant (Table 1).

The above results suggest a direct interaction of E41 with the nitroxide, possibly a H-bonding or electrostatic interaction. Indeed, substitution of E41 by aspartate produces a significant increase in the immobilized component (Figure 6E). The spectrum can be closely fit with two states similar to those of 52R1 with WT neighbors, but with an increase in occupancy of the immobilized state from 12 to 39% and a decrease in S_{20} of the ordered state (Table 2).

If we assume that the two dynamic components of the R1 side chain arise from two rotamers of R1 in slow exchange on the EPR time scale, the equilibrium constant and free energy difference between them can be estimated from the populations given in Table 2. For 52R1, the free energy of the immobilized rotamer lies ~1 kcal/mol higher in energy relative to the ordered state. In E41D/52R1, the immobilized rotamer lies only ~0.3 kcal/mol above the ordered state. Thus, the strength of the apparent nitroxide/carboxylate interaction has increased about 0.7 kcal/mol in the E41D/52R1 mutant.

In addition to a H-bonding/electrostatic interaction, van der Waals interactions can also occur between 52R1 and the HB neighbor at 41. For example, substitution of E41 by tryptophan results in a two-component spectrum that closely resembles that of 116R1, where the native residue at the HB site is also tryptophan (compare Figures 5F and 7F). One component of high occupancy is strongly immobilized, with a correlation time similar to that for the overall rotation of the entire protein.

Mutation of the Non-Hydrogen-Bonded Neighbor, I61. Substitutions at the NHB neighbor 61 also produce large changes in 52R1 mobility, suggesting important side-chain interactions. Figure 8A shows again the spectrum of 52R1 with the native neighbors for reference. Figure 8B shows the remarkable effect of replacing the native β-branched isoleucine side chain with leucine. The immobilized component, tentatively assigned to interaction of R1 with E41, disappears. The spectrum of 52R1/I61L can be fit by a single population undergoing anisotropic motion similar to that of the ordered state in 52R1, but with a reduced order parameter of $S_{20} = 0.50$. When I61 was replaced by either of two other β-branched residues, valine or threonine, a two-component spectrum characteristic of 52R1 resulted. In each case, the immobilized component is again present with properties similar to that in the spectrum of 52R1, although it is present in larger proportion (Figure 8C,D, Table 2). The more mobile component has the same anisotropic motion as the ordered component in 52R1. For valine, the order parameter is about the same as that for 52R1, while it is decreased for the threonine substitution (Table 2). These data demonstrate the importance of the β-branch at 61 in producing a constrained environment that gives rise to a highly ordered motion of R1. As will be discussed further below, it is likely that the immobilizing interaction with E41 is favored only in highly

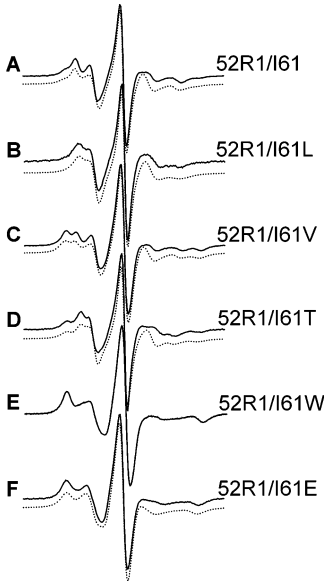

FIGURE 8: EPR spectra of CRBP 52R1 with the indicated side-chain substitutions for NHB neighbor I61. The solid traces are experimental spectra, and the dotted traces are the least-squares best fits to the MOMD model (see Methods). At high concentrations, the spectrum of (B) was concentration-dependent, suggesting oligomerization. The spectrum shown was recorded in dilute solution, where the line shape was concentration-independent.

ordered states, because the entropy loss upon immobilization is reduced.

Finally, Figure 8E,F shows the effect of replacing I61 by tryptophan and glutamate, respectively. Replacement by tryptophan gives rise to a spectrum of 52R1 similar in type to that found for 116R1 with a native tryptophan at the HB site, and for 52R1 with tryptophan substituted at the HB neighbor E41. Each is characterized by a population of strongly immobilized nitroxide. Interestingly, replacement of I61 by glutamate gives rise to a dominant population of an immobilized component in the spectrum of 52R1 (60%).

Collectively, the above results suggest that a β-branched residue at the NHB neighbor site produces a highly ordered state, and thus it cooperates with the carboxylate at the HB site to produce an immobilized component. Because the β-branch projects toward or away from R1, depending on whether it is at the NHB or HB site, respectively (Figure 6), the interaction should not be symmetric with respect to exchange of neighbors. This is confirmed by comparison of the spectra for 52R1 with native neighbors and for the "exchanged" mutant E41I/52R1/I61E (Figure 9A,B). On the other hand, for 52R1 without a β-branched residue at the NHB site, the motion is roughly symmetric with respect to neighbor exchange (compare Figure 9C,D).

Interactions of 54R1: Comparison with 52R1. Although 54R1 is the next solvent-exposed residue along the same strand that contains 52R1, the EPR spectra, and hence motions of the side chains, are very different. For reference, Figure 10A shows a direct comparison of the EPR spectra for these two sites. The spectrum of 54R1 can be fit to an anisotropic motion similar to that for the ordered component of 52R1, but with much lower order ($S_{20} \approx 0.35$; Figure 5, Table 2). The presence of the β-branched residue at the NHB site in 52R1 cannot entirely account for the difference in side-chain ordering, as shown by comparison of the 54R1 spectrum with 52R1/I61L, where the β-branched residue has

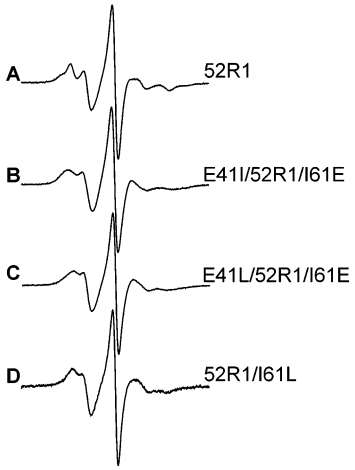

FIGURE 9: EPR spectra of CRBP 52R1 and indicated mutants that exchange the HB and NHB neighbors.

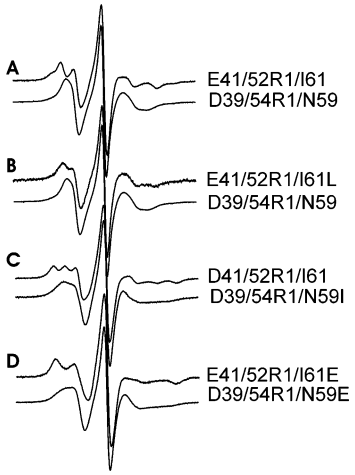

FIGURE 10: EPR spectra of CRBP 52R1, CRBP 54R1, and the indicated mutants thereof that isolate the effect of strand geometry of side-chain motion.

been replaced by a linear one (Figure 10B). As is evident, the order of the 52R1/I61L ($S_{20} \approx 0.5$) still exceeds that of 54R1. The fact that the difference in motion of 52R1 and 54R1 is not due entirely to the identity of the neighboring side chains is dramatically illustrated in the "transmutation" experiment of Figure 10C, wherein mutants of 52R1 and 54R1 were created that had identical NHB and HB neighbors. Again, the spectra remain distinct, pointing to additional effects that must give rise to the distinction.

As shown in Figure 4A, residue 54 has a significant twist relative to 52. As will be discussed in detail below, this causes the side chain of 54 to angle away from the NHB neighbor site in β4, presumably resulting in a reduced interaction, thus offering a simple explanation for the generally lower order for the motion of 54R1 compared to that of 52R1 (Table 2). Further evidence for the reduced interaction of 54R1 with the NHB neighbor relative to 52R1 is provided in Figure 10D, which shows the much-reduced effect of a glutamate residue at the NHB site on the motion of 54R1 compared to 52R1.

Interactions of 116R1. Residue 116R1 is located in β9 of the β8$-\beta$10 sheet that has a right-handed twist (Figure 4), and it was selected for study to elucidate the origin of the strong immobilization and examine potential effects of sheet twist. For reference, Figure 11A shows the spectrum of

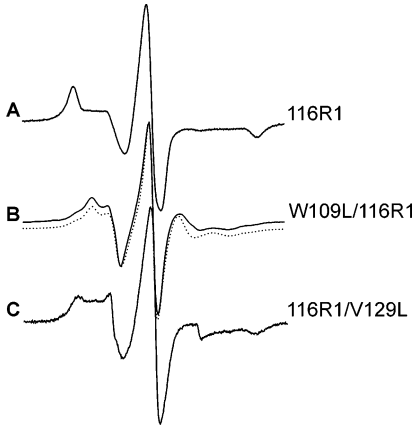

FIGURE 11: EPR spectra of CRBP 116R1 with indicated side-chain substitutions for HB and NHB neighbors. The solid traces are experimental spectra, and the dotted trace in (B) is the least-squares best fit to the MOMD model (see Methods).

116R1 with native HB and NHB neighbors, W109 and the β-branched V129, respectively. Figure 11B shows that replacing the tryptophan by leucine dramatically reduces the most immobilized component, but the motion of the dominant population of 116R1 is still highly ordered in this mutant ($S_{20} \approx 0.5$; Table 2), with a motion very similar to that of 52R1/I61L ($S_{20} \approx 0.5$; Table 2).

The β-branched NHB neighbor of 116R1 has only a minor role in the immobilization of 116R1, as shown by the spectrum in Figure 11C for the mutant 116R1/V29L, which is very similar to that for 116R1 itself. The data of Figure 11, together with those of Figures 7F and 8E, clearly illustrate the direct or indirect interaction of R1 with tryptophan at either the HB or NHB site. Models for this interaction will be considered below.

R1 Motions at Solvent-Exposed Sites in Edge Strands β4, β5, and β6. Strands β4, β5, and β6 and the C-terminal half of strand β1 are "edge" strands with hydrogen bonds to an adjacent strand only on one side (Figure 3). The spectra of R1 at sites in these strands are shown in Figure 12. Collectively, the spectra reflect much more homogeneous motions compared to those for R1 in center strands (Figure 5), with all but one (81R1) reflecting a single dynamic mode.

Most striking are the spectra of R1 in β4 (59, 61, 63) and at 71 in β5, where the line shapes are all similar to that for R1 at a solvent-exposed site in a rigid helix, such as 72R1 in T4L (Figure 1C). Indeed, they all can be fit with parameters similar to those for the T4L 72R1 spectrum (Figure 12, dotted traces; Table 2), suggesting a similar anisotropic motion for each of these side chains (*4*). A model for the structural origin of this anisotropic motion at β-edge strands will be presented in the Discussion.

Although the EPR spectra for residues 14R1 (in β1) and 73R1 (in β5) appear quite different from those of R1 at the other edge strand sites, they in fact are best fit with the same anisotropic motion with similar rates, but with reduced order parameters (Table 2). For example, 14R1 and 73R1 both have $S_{20} \approx 0.3$, compared to $S_{20} \approx 0.5$ for 59, 61, 63, and 73. This difference in S_{20} corresponds to a difference of only $\sim$7° in the mean angle of motion of the nitroxide 2p orbital and underscores the extreme sensitivity of the EPR line shapes to detect small differences in motion. This relatively small difference could be accounted for by contributions from backbone fluctuations in 14 and 73, the last residues in β1 and β6, respectively.

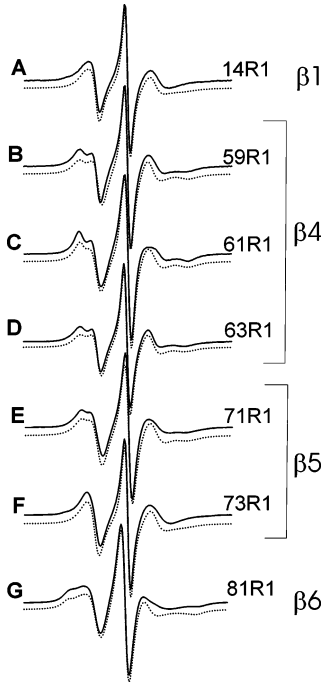

FIGURE 12: EPR spectra of R1 at the indicated sites in edge strands of CRBP. The solid traces are experimental spectra, and the dotted traces are the least-squares best fits to the MOMD model (see Methods).

Finally, residue 81R1 has a complex (multicomponent) spectrum suggestive of interactions of the nitroxide with the environment. The nitroxide ring of 81R1 is within interaction range of a cluster of three acidic residues, namely D71, D73, and E100. Considering the interactions identified above for 52R1 with E41, a COO^-/nitroxide interaction is a possibility for the origin of the more immobilized component in the spectrum of 81R1.

R1 Motions at Sites Facing the Ligand-Binding Cavity. Figure 13 shows the spectra of R1 residues at buried sites in β1 (13), β3 (60, 62), and β9 (117, 119, 121). These spectra reflect a strongly immobilized nitroxide. Using the maximum hyperfine splitting to estimate the correlation time of the nitroxide according to the simplified method of Freed (*27*), 60R1 and 62R1 are found to have $\tau_c \approx 14$ ns, close to the correlation time for rotary diffusion of CRBP itself in solutions of 30% sucrose ($\tau \approx 20$ ns at 295 K). Within the error of these estimates, it can be concluded that the buried nitroxides at sites 60 and 62 are essentially immobilized with respect to the protein, as expected. Considering the similarity in line shapes for the other buried residues, similar correlation times would be expected.

Figures 5, 12, and 13 together provide the data for continuous R1 scans through β4 and β9. In previous work, it was found that the inverse of the line width of the center line of the nitroxide spectrum (ΔH_0^{-1}) provides a semiquantitative measure of nitroxide mobility. Figure 14A,B shows plots of this parameter along the sequences of β4 and β9, and the periodicity of 2 characteristic of the β conformation is evident.

The solvent accessibility of the R1 side chain in a protein can be estimated from the collision rate of the nitroxide with paramagnetic reagents in solution (*24*). Molecular oxygen

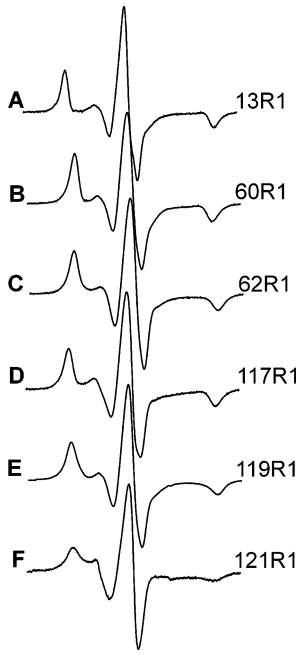

FIGURE 13: EPR spectra of R1 at the indicated buried sites in CRBP.

and Ni(EDDA) are commonly used reagents for this purpose, and the corresponding collision parameters, proportional to the collision rates, are designated $\Pi(O_2)$ and Π(NiEDDA). Figure 14 also includes the sequence dependence of these parameters, and it is evident that the periodicity matches that of the mobility. These data make a convincing argument that the presence of the nitroxide side chain produces little perturbation of the protein fold.

DISCUSSION

In earlier studies, it was found that the EPR spectra of R1 in α-helical proteins could be understood in terms of the rotamer structure and a simple model for the internal motion of the side chain (Figure 1). The internal motion is modulated by protein backbone fluctuations and interactions of the nitroxide with the environment to generate a variety of complex line shapes that can be deciphered to some extent in terms of protein structure and dynamics.

The salient features of the spectral line shapes observed in β structures can also largely be rationalized in terms of a simple model for the side-chain rotamers. However, unlike the case for helices, the rotamer states for side chains in β-sheets are dictated by steric interactions with nearest neighbors. In describing the model, the m, p, t rotamer designation of Lovell et al. is adopted to avoid the confusion that exists regarding the definition of g^+ and g^- states (*28*). The convention is illustrated in Figure 6 and described in the legend, and will be used to designate both χ_1 and χ_2 dihedrals of R1. Thus, rotamers will be designated as {m,p}, for example.

For R1 at solvent-exposed sites in α-helices, both the {m,m} and the {t,p} states are observed in crystal structures of spin-labeled T4L, with the former apparently being preferred (*3*; M. Fleissner, M. Sawaya, D. Cascio, and W. Hubbell, unpublished data; Z.Guo, D. Cascio, and W. Hubbell, unpublished data). In both of these states, the S_δ atom is within ~3−3.75 Å of the $C_\alpha H$ hydrogen atom.

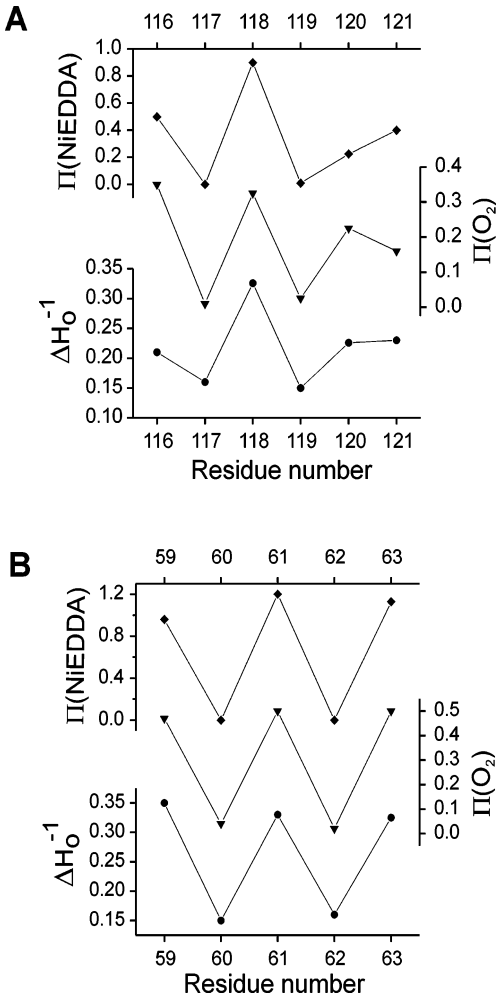

FIGURE 14: Plots of ΔH_o^{-1}, $\Pi(O_2)$, and Π(NiEDDA) through β4 (A) and β9 (B).

Because there is no other obvious energetic reason to prefer the {m,m} or {t,p} states over the {m,t} or {t,t}, where the S_δ is moved away from the backbone, the data suggest an attractive interaction between the S_δ and hydrogen atoms. It is interesting to note that, in an early study, Scheraga reported a similar interaction in disulfide bridges (*29*). In surveying the much larger current database, Petersen et al. in 1999 confirmed the strong dominance of the {m,m} state for disulfides (*30*).

The apparent S_δ−backbone interaction is a central feature in determining the motion of the nitroxide ring, and hence the EPR spectrum, because it greatly reduces the number of degrees of freedom for the internal motion (*4*). In the absence of other interactions, such as the *syn*-pentane effect (*31*) or tertiary contacts, the {m,m}and {t,p} states will be taken as the preferred states of R1, independent of secondary structure. In interior strands of β-sheets, the p state of χ_1 for R1 is not favorable, due to direct steric clash of R1 with the HB neighbor. Only at edge strands missing the HB neighbor is the p state possible. Thus, in modeling R1 in CRBP in interior strands, only m and t states for χ_1 are considered.

Motion of R1 at Solvent-Exposed Sites in an Interior Strand of a Flat Sheet. Consider first the R1 side chains at solvent-exposed sites in center strands with no twist. This situation is represented by residues 50 and 52 in strand β3. The EPR spectrum of 50R1 (Figure 5B) is best fit with two

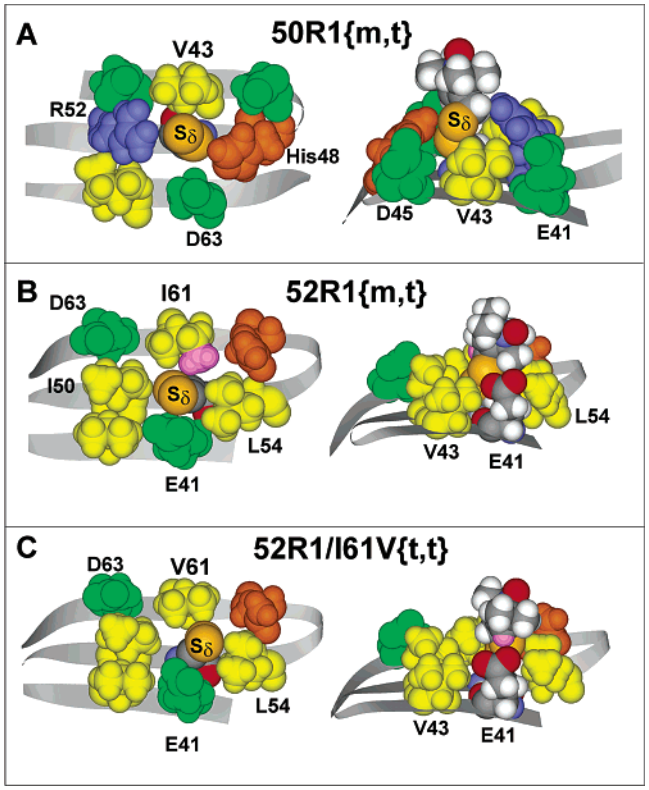

FIGURE 15: Molecular models of 50R1 (A), 52R1 in the {m,t} configuration (B), and 52R1/I61V in the {t,t} configuration (C). In each, the left-hand panel is a top view, looking nearly down the disulfide axis, with the nitroxide group removed. The right-hand panel is a side view, with the nitroxide in place. Side chains are color-coded as follows: hydrophobic, yellow; acidic, green; glutamine, asparagine, histidine, orange; threonine, cyan; tryptophan, magenta. In (B) and (C), right-hand panels, HB neighbor E41 is colored according to atom type. In (C), right-hand panel, the 4H atom of the nitroxide ring is colored magenta.

components (Table 2), but the component with $\tau \approx 2.2$ ns, $S_{20} \approx 0.27$ strongly dominates (90%). This rate is similar to R1 at the solvent-exposed helix site T4L 72R1 ($\tau \approx 2.1$ ns, $S = 0.47$), but the order is significantly less, and this is clearly reflected in the difference in the respective EPR spectra (Figures 1C and 5B). The reduced order in the motion of 50R1 relative to T4L 72R1 can be understood in terms of the local structure around the site in the interior of a flat β-sheet, where the $C_\alpha - C_\beta$ bond vector lies roughly parallel to those of its neighbors. This geometry creates a sufficiently crowded environment where the favored rotamers, {m,m} and {t,p}, cannot be formed due to severe steric clashes with the NHB site, the closest neighbor. Rather, the side chain is forced into the {m,t} or possibly the {t,t} state, where the S_δ sulfur of the disulfide cannot contact main-chain atoms, and the interaction that gives rise to the ordered motion at helical sites is lost. Instead, the S−S bond projects away from the backbone.

A model of 50R1 in the {m,t} configuration is shown in Figure 15A. The left panel shows a top view with the nitroxide ring removed, so the environment of the nearly vertical disulfide is clearly seen. Although the environment is crowded enough to prevent formation of {m,m} and {t,p} rotamers, there is sufficient room to allow torsional oscillations about χ_1 and χ_2 that are damped at α-helical sites due to interaction of S_δ with the backbone. This accounts for the rather paradoxical result that the more crowded environment at a β-sheet site results in a less ordered motion at 50R1. The right panel in Figure 15A shows a side view of the site, viewed from the HB neighbor, showing that the nitroxide itself projects beyond the neighboring side chains, allowing relatively free motion about χ_4 and χ_5. The {t,t} rotamer can also be formed in 50R1 and leads to conclusions similar to that for the {m,t} state.

Interestingly, the next residue along the strand, 52R1, has a complex spectrum that reflects two dynamic states of the side chain (Figure 5C). Unlike 50R1, the dominant state (90%) has a strongly ordered motion ($\tau \approx 1.3$ ns, $S_{20} \approx 0.7$), the order parameter of which exceeds that for T4L 72R1. The minor population is immobilized, with a correlation time roughly equal to that for the rotary diffusion of CRBP. What is the structural origin of the highly ordered state? The data of Figure 8 show that a β-branched residue at the NHB position is necessary for the highly ordered motion. This result can be rationalized in terms of the model shown in Figure 15B. The left panel again shows a top view with the nitroxide removed, with R1 in the {m,t} configuration. A comparison with Figure 15A, left panel, clearly shows that the environment around the disulfide of 52R1 is more crowded. The bulky β-branched isoleucine residue at NHB neighbor 61 makes contact with the disulfide and greatly reduces the volume in which the disulfide can move. It is likely that the E41 HB neighbor also contributes to constraining the disulfide by direct interaction (as can be seen in Figure 15), because substitution of E41 leads to a reduction in S_{20} of the ordered component (Figure 7, Table 2), in addition to causing loss of the minor immobilized component. In addition, L54 can apparently make contact with 52R1 because the terminal end of β-strand 3 curves upward, causing L54 to project toward 52 (see Figure 4). Taken together, these interactions strongly constrain the motion of the disulfide, giving rise to the highly ordered motions observed. It is important to note that β-branched residues have an effect only at the NHB site, because at the HB site the branch substituents point away from the residue. This is shown most clearly by the fact that "swapping" NHB and HB neighbors has a strong effect when one is branched, but little if neither is branched (Figure 9).

The results of the systematic mutagenesis of the HB neighbor of 52 (E41), shown in Figure 7, suggest that the minor, strongly immobilized component arises from a polar interaction (H-bonding; electrostatic) with the nitroxide. Thus, replacement of E41 by glutamine, lysine, or threonine essentially eliminates the immobilized component, whereas replacement by aspartate increases the interaction. Moreover, substitution of the NHB neighbor with glutamate, so that both neighbors bear carboxylate groups, makes the immobilized state dominant (Figure 8F). Crystal structures of the T4L mutant 75R1 revealed an unusual C—H···O hydrogen bond between tyrosine and the 4H atom on the nitroxide ring. One of several possibilities for the interaction is then a similar hydrogen bond to glutamate in place of tyrosine. This possibility is modeled in Figure 15C, right panel, for the E41/52R1 interaction.

The β-branched residues valine and threonine also produce a strongly ordered state when substituted at 61, and result in an increase in the immobilized population. Consider the valine substitution that produces a dramatic increase in the

population of the immobilized state from 6 to 43%, while the strongly ordered state is about the same as for isoleucine ($S_{20} \approx 0.71$). This interesting result may serve to identify the rotamer of R1 that corresponds to the immobilized state. Figure 15B,C compares the structures around site 52 for I61 and the I61V mutation. For I61, the favored rotamer is clearly {m,t}, because in the other possible state, {t,t}, direct steric clash of the S_δ occurs with the C_δ carbon of isoleucine (colored magenta in Figure 15B). On the other hand, Figure 15C shows that, in I61V, the {m,t} and {t,t} rotamers are equivalent, due to the symmetrical structure of valine (the {t,t} state in I61V has the same structure shown in Figure 15B). Thus, it is likely that the {t,t} rotamer is the one in which the nitroxide interaction occurs with E41. Indeed, the model in Figure 15C, right panel, shows that in the {t,t} state, the 4H atom of the nitroxide ring is in close apposition to the E41 carboxylate. It is also evident that the opportunity exits for several hydrophobic interactions. Within the context of this model, the two dynamic states of 52R1 then represent an equilibrium between the {m,t} and {t,t} configurations.

Substitution of threonine, which is nearly isosteric with valine, should produce a similar effect when substituted at 61, and indeed this is the case. The I61T mutant results in an increase of the immobilized component from 6 to 34%, but the ordered state has a lower order ($S_{20} = 0.56$) compared to valine or isoleucine. This could be accounted for by a reduced van der Waals interaction of an $-$OH group with the S_δ sulfur compared to a $-CH_3$ group.

The data of Figure 8 show that a β-branched residue at the NHB position gives rise to a highly ordered state and is necessary to observe the immobilized component. The reason the constraining interaction of the β-branched residue is required for the immobilized component is a matter of speculation. The proposed interaction with nitroxide ring that produces the immobilized state is a weak one. Using the populations estimated from spectral simulation of 52R1 given in Table 1, the free energy of forming the immobilized component from the ordered rotamer is $\sim +1$ kcal/mol. Thus, the enthalpy difference of the immobilizing interaction is insufficient to overcome the entropy loss. In this case, the entropy loss from a less ordered state, such as that for R1 in the presence of a nonbranched residue at the NHB site, would make the free energy change so unfavorable that the interaction may not be observed.

Residues 48 and 54 are of interest, because they are the first and last residues in β3 and have positive twists ($\varphi + \psi > 0$, where φ and ψ are the backbone dihedral angles) that distinguish them from other residues in the strand (Figure 4A). The EPR spectrum of 48R1 is complex and best fit by two components, both weakly ordered. The dominant component has a correlation time $\tau \approx 5$ ns. Because the intrinsic correlation times for the nitroxide motion due to oscillation about internal bonds apparently lie in the range of 1$-$2 ns (*4*), this slow motion may arise from fast exchange between states having weak interactions of the nitroxide ring. Figure 16A shows a model of 48R1 in the {t,t} state, where possible hydrophobic interactions can occur with V43, as well as a possible H-bonding interaction with D48. Although the NHB neighbor (Q65) projects away from 48R1, steric clash of the S_δ with Q65 is still sufficient to preclude formation of the {m,m} conformation. Nevertheless, the site

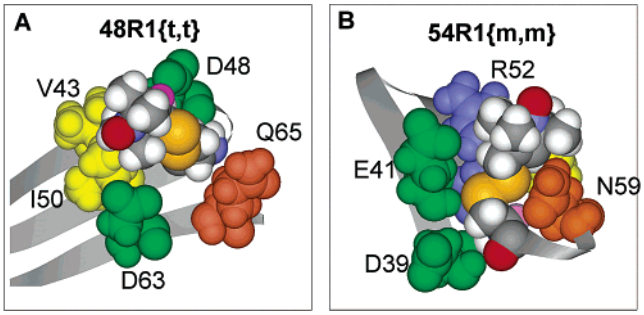

FIGURE 16: Models of 48R1 (A) and 54R1 (B) in the {m,t} and {m,m} conformations, respectively. The color code for the amino acids is the same as in Figure 15.

is relatively open, allowing motion of the entire R1 side chain.

The EPR spectrum of 54R1 reflects an anisotropic, weakly ordered ($S_{20} = 0.35$) motion characteristic of R1 at solvent-exposed α-helical sites. The origin of this motion can be understood in terms of the topology of the protein around the site. The positive twist of 54 causes the side chain to point away from the NHB neighbor N59 (Figure 6), relieving steric constraints and allowing the formation of the preferred {m,m} conformation, as shown in the model in Figure 16B. As mentioned above, in this rotamer the S_δ atom can make contact with the $C_\alpha H$ hydrogen (magenta in Figure 16B), constraining the disulfide and giving rise to the anisotropic motion. Thus, the motion of R1 is strongly dependent on the topology of the sheet, a result that is further emphasized in the "transmutation" experiments shown in Figure 10.

Motion of R1 at Solvent-Exposed Sites in the Interior Strand of a Twisted Sheet. The sheet containing β9 is characterized by a right-handed twist. The twist in the individual strands near the site of interest determines the proximity of the important NHB neighbor and the preferred rotamer about χ_1, χ_2. For example, the twist in β10 causes NHB neighbors to point away from residues 114 and 116, and to a lesser degree, away from 118 and 120. These features can be qualitatively appreciated from Figure 4B. Figure 17A$-$D shows models of R1 at 114, 116, 118, and 120, respectively. In each, the left-hand panel is a top view with the nitroxide removed. As can be seen, the twist of adjacent strand β10 allows sufficient room to form the {m,m} rotamer at 114 and 116, but not at 118 and 120, where only the {m,t} state can be formed due to steric clash of the S_δ with the NHB neighbor in the {m,m} state. The right panel in each shows a side view displaying the environment around the nitroxide ring.

In the {m,m} state of 114 and 116, the disulfide contacts main-chain atoms, constraining motion of the disulfide. In addition, the nitroxide ring is closer to the backbone, creating an opportunity for interactions with neighboring side chains. In the {m,t} state of 118 and 120, the disulfide cannot contact the backbone, and the nitroxide projects above the level of the neighboring side chain, giving rise to greater motional freedom.

The EPR spectra of these residues are qualitatively in harmony with the models. Thus, 114 and 116 have ordered and immobilized R1 side chains, respectively, while 118 and 120 have highly mobile R1 side chains. In 114R1, the dominant spectral component has an order parameter of $S_{20} \approx 0.58$, likely due to constraints on the disulfide arising from

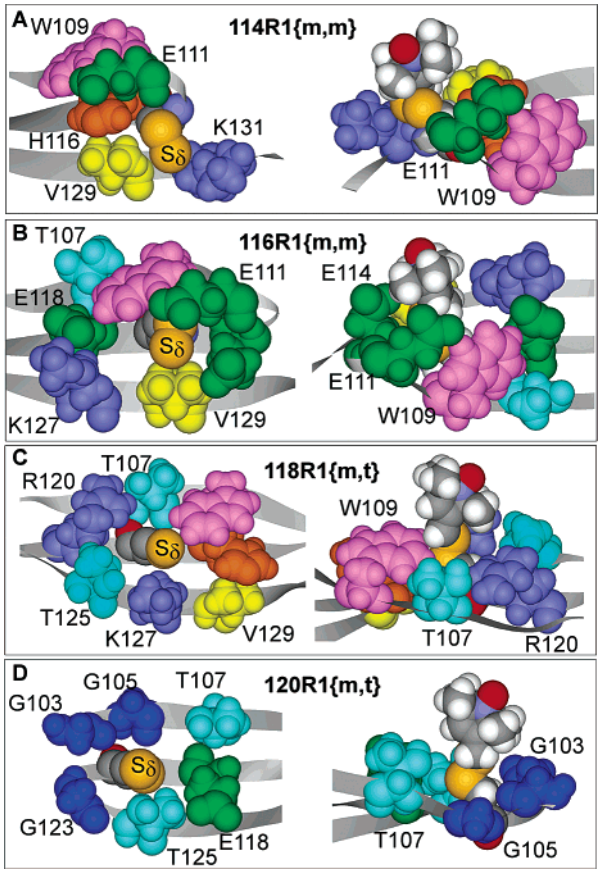

FIGURE 17: Molecular models for the solvent-exposed residues in β9. In each part, the left-hand panel shows a top view of the sheet, with the nitroxide removed. The right-hand panel shows a side view with the nitroxide ring in place. The color code is the same as in Figure 15.

a combination of the interaction of the backbone and the NHB side chain (Figure 17A, left panel). This degree of order is similar to that seen in various E41 mutants of 52R1. Although the R1 rotamers are different, the fundamental origin of the order is the same, namely constraints on the disulfide. The second component of 114R1 is highly mobile, with essentially no ordering. This may arise from the existence of a second rotamer, possibly {m,t}, which is readily formed.

The EPR spectrum of 116R1 is dominated by a highly immobilized state. Site 116 is a special case due to the presence of W109, which provides a highly constrained environment (Figure 17B). Not only is the disulfide highly constrained due to interactions with the backbone and V129, but also the nitroxide can make multiple contacts with neighboring residues, two of which are glutamates (111, 114). Mutation of W109 to leucine results in a dramatic reduction of the strongly immobilized component. Simulations (Figure 11, Table 2) show that an immobilized state is now only 10% occupied, and the dominant state has an ordered motion similar to that of 114R1. In the native structure, W109 is salt-bridged/H-bonded to E111, the residue that makes the most extensive contacts with the nitroxide (Figure 17B). Removal of W109 would allow repositioning of 111, and consequent loss of interaction with 116R1. In addition, it is interesting to note that the most commonly observed neighbor of half-cystine residues in proteins is tryptophan, suggesting an attractive aromatic−disulfide interaction (*30*, *32*). Indeed,

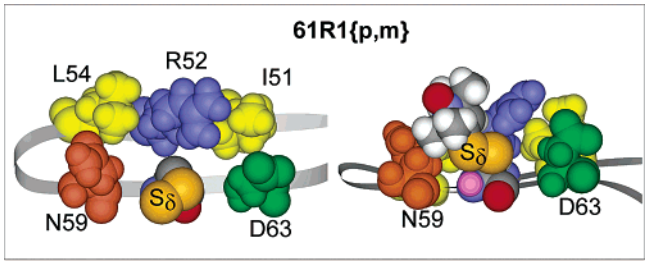

FIGURE 18: Molecular model of the edge strand residue 61R1. The left-hand panel has the nitroxide removed, viewed from the top. The right-hand panel is a side view, including the nitroxide ring.

the model in Figure 17B shows the direct contact of the S_γ sulfur with W109. The ordering of the 116R1 side chain in the W109L mutant is essentially that expected on the basis of the disulfide−backbone interaction in the {m,m} state. The small, immobilized component in W109L could arise from interactions with nearby glutamates 111 and/or 114.

Simulations of the EPR spectrum for 118R1 suggest a low ordering of the side chain ($S_{20} \approx 0.2$), consistent with the model of the {m,t} state shown in Figure 17C. In this state, interactions of the disulfide with the backbone are absent, and some motion about χ_1, χ_2 is allowed. Here, the nitroxide ring projects well above the level of the nearest side chains, and torsional oscillations about χ_4, χ_5 would be unimpeded by tertiary interactions. The very mobile state of 120R1 can be accounted for in the same terms. In this case, the motional freedom is expected to be even greater due to the presence of three glycine residues among the nearest neighbors.

Motion of the R1 Side Chain at Solvent-Exposed Sites in Edge Strands. Residues in edge strands β1, β4, β5, and β6 were investigated. The most striking pattern of motions is revealed in the EPR spectra of R1 in β4 and β5, where the line shapes reveal an anisotropic, ordered motion very similar to that observed for R1 in α-helices (Figure 12). As described above, this motion occurs in rotamers where the disulfide is relatively immobilized, either by constraints imposed by the environment, as in 52R1, or by interaction with main-chain atoms, as in 54R1, 114R1, and in α-helices.

The solvent-exposed edge strand sites are unique in that they are missing the neighbor at the HB site. At each site, the NHB neighbor lies in close proximity, precluding the formation of the {m,m} state. As shown in Figure 18, this situation should favor {p,m} or {p,t} rotamers, where the disulfide projects directly toward the missing HB neighbor. In the {p,m} state, shown in the figure, the S_δ atom approaches the NH hydrogen within about 3 Å, the same distance as that between S_δ and the $C_\alpha H$ hydrogen in the {m,m} state. Assuming a similar attractive interaction, the disulfide would be constrained, accounting for the experimental results. Indeed, the order parameters for R1 at 59, 61, 63, and 71 are all about $S \approx 0.48$, identical to that for R1 at T4L 72R1. In the {p,t} rotamer, one would expect a more mobile, less ordered state, perhaps like that of 118R1.

Interestingly, the spectra of 14R1 and 73R1 have very low order ($S_{20} \approx 0.3$ for each), even though the same {p,m} rotamer can be formed as for the ordered R1 residues discussed above. It is likely that this can be accounted for on the basis of backbone motion. Indeed, both 14 and 73 have S^2 values for the NH bond vector significantly below the average value of other residues in edge strands in CRBP,

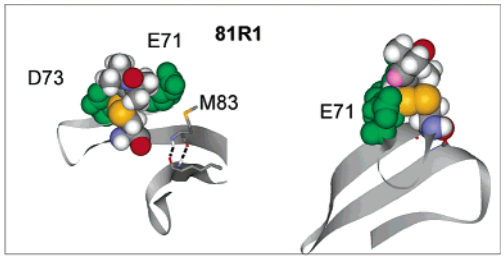

FIGURE 19: Molecular model of edge strand 81R1, showing possible origins of interactions. The dashed lines show backbone H-bonds, illustrating that 81 is the final residue that can be considered an edge strand.

as determined by ^{15}N NMR relaxation methods (*12*). It is of interest to note that the difference in order parameter for the nitroxide ring between the ordered sites in edge strands β4 and β5 ($S_{20} \approx 0.48$) and in 14 and 73 ($S_{20} \approx 0.3$) corresponds to a difference in the mean angle of fluctuation of the 2p orbital of the nitroxide of only ~5°. For comparison, the mean angular difference for the NH bond vector motion between residue 14 and the average value for residues in β4 and β5 is ~3°.

The spectrum of 81R1 requires two components for a reasonable simulation (Figure 12G). The dominant component (70%) appears to be in relatively rapid motion and weakly ordered ($\tau \approx 3.7$ ns, $S_{20} \approx 0.33$), while the second component has a slightly slower rate and a high order ($\tau \approx 5$ ns, $S_{20} \approx 0.57$). At site 81, due to strand twist, the NHB neighbor (D71) points away from 81R1, allowing the formation of the {m,m} state in addition to the {p,m} state (Figure 19). In either case, immobilization of the disulfide is expected. However, in the {m,m} state, the nitroxide is placed in direct interaction with aspartates 71 and 73, and a possibility exists for formation of a C—H···O bond between the 4H on the nitroxide ring and a COO^- group, which could give rise to the more highly ordered component. The EPR spectrum could then be understood in terms of equilibrium between the two possible rotamers.

SUMMARY AND CONCLUSIONS

The data and discussion presented above suggest a simple working model for understanding the EPR spectra, and hence the dynamics, of the R1 nitroxide side chain in β-sheet proteins. The single most important feature of the model is the interaction of the R1 disulfide with the NHB neighbor. In interior strands of flat sheets, the proximity of the NHB neighbor prevents formation of the preferred {m,m} conformation of the side chain due to steric clash with S_δ, allowing only the {m,t} state and possibly the {t,t} state. The p state ($\chi_1 = +60$) cannot occur, due to direct steric clash with the HB neighbor. In the {m,t} or {t,t} states, the disulfide projects directly outward from the backbone, placing the nitroxide generally above the level of the neighboring side chains. If the NHB neighbor is β-branched, steric crowding of the site constrains the disulfide, and a highly ordered motion can result. If the NHB neighbor is linear, sufficient motion of the disulfide occurs to lead to a weakly ordered state. Twisting of the strand can reduce the interaction of R1 with the NHB neighbor, leading to an increase in mobility. In particular, this situation can permit the formation of the favored {m,m} state, wherein a weakly ordered motion occurs similar to that for R1 at solvent-exposed helix sites.

In a highly ordered state, weak interactions of the nitroxide ring with nearest neighbors can occur, leading to relative immobilization of the nitroxide with respect to the protein. In the present work, an apparent interaction with a carboxylate group was identified at site 52, and similar interactions were implicated in the immobilization at several other sites.

At solvent-exposed sites in edge strands where the HB neighbor is missing, the {p,m} and {m,t} states are possible. For such sites, the nitroxide motion is ordered, apparently due to constraints on the disulfide motion due to interaction with main-chain atoms. Again, strand twisting can reduce interactions with the NHB neighbor, permitting the {m,m} state to become occupied.

The validity of this working model remains to be tested through the determination of crystal structures of suitable spin-labeled proteins. Under any circumstances, it is apparent that R1 motion in β-strands is strongly modulated by side-chain interactions. Given the extreme sensitivity of the EPR spectra to side-chain motion, and the dependence of side-chain interactions on strand twisting, it seems likely that SDSL will be a useful approach for monitoring conformational changes in β-proteins.

ACKNOWLEDGMENT

We thank Dr. Christian Altenbach for scientific and technical assistance and Dr. Linda Columbus for many helpful discussions.

REFERENCES

1. Mchaourab, H. S., Lietzow, M. A., Hideg, K., and Hubbell, W. L. (1996) Motion of spin-labeled side chains in T4 lysozyme. Correlation with protein structure and dynamics, *Biochemistry 35*, 7692−7704.
2. Mchaourab, H. S., Kálai, T., Hideg, K., and Hubbell, W. L. (1999) Motion of spin-labeled side chains in T4 lysozyme: effect of side chain structure, *Biochemistry 38*, 2947−2955.
3. Langen, R., Oh, K. J., Cascio, D., and Hubbell, W. L. (2000) Crystal structures of spin labeled T4 lysozyme mutants: implications for the interpretation of EPR spectra in terms of structure, *Biochemistry 39*, 8396−8405.
4. Columbus, L., Kálai, T., Jekö, J., Hideg, K., and Hubbell, W. L. (2001) Molecular motion of spin labeled side chains in alpha-helices: analysis by variation of side chain structure, *Biochemistry 40*, 3828−3846.
5. Columbus, L. and Hubbell, W. L. (2002) A new spin on protein dynamics, *Trends Biochem. Sci. 27*, 288−295.
6. Isas, J. M., Langen, R., Haigler, H. T., and Hubbell, W. L. (2002) Structure and dynamics of a helical hairpin and loop region in annexin 12: a site-directed spin labeling study, *Biochemistry 41*, 1464−1473.
7. Salwiński, L., and Hubbell, W. L. (1999) Structure in the channel forming domain of colicin E1 bound to membranes: the 402−424 sequence, *Protein Sci. 8*, 562−572.
8. Hubbell, W. L., Cafiso, D. S., and Altenbach, C. (2000) Identifying conformational changes with site-directed spin labeling, *Nat. Struct. Biol. 7*, 735−739.
9. Berengian, A. R., Bova M. P., and Mchaourab, H. S. (1997) Structure and function of the conserved domain in alphaA-crystallin. Site-directed spin labeling identifies a beta-strand located near a subunit interface, *Biochemistry 36*, 9951−9957.
10. Klug, C. S., Su, W., and Feix, J. B. (1997) Mapping of the residues involved in a proposed beta-strand located in the ferric enterobactin receptor FepA using site-directed spin-labeling, *Biochemistry 36*, 13027−13033.
11. Cowan, S. W., Newcomer, M. E., and Jones, T. A. (1993) Crystallographic studies on a family of cellular lipophilic transport proteins. Refinement of P2 myelin protein and the structure

determination and refinement of cellular retinol-binding protein in complex with all-trans-retinol, *J. Mol. Biol. 230*, 1225−1246.
12. Franzoni, L., Lücke, C., Pérez, C., Cavazzini, D., Rademacher, M., Ludwig, C., Spisni, A., Rossi, G. L., and Rüterjans, H. (2002) Structure and backbone dynamics of apo- and holo-cellular retinol-binding protein in solution, *J. Biol. Chem. 277*, 21983-21997.
13. von Heijne, G., and Blomberg, C. (1977) The beta structure: inter-strand correlations, *J. Mol. Biol. 117*, 821−824.
14. Lifson, S., and Sander, C. (1980) Specific recognition in the tertiary structure of beta-sheets of proteins, *J. Mol. Biol. 139*, 627−639.
15. Minor, D. L., and Kim, P. S. (1994) Context is a major determinant of beta-sheet propensity, *Nature 371*, 264−267.
16. Wouters, M. A., and Curmi, P. M. G. (1995) An analysis of side chain interactions and pair correlations within antiparallel beta-sheets: the differences between backbone hydrogen-bonded and non-hydrogen-bonded residue pairs, *Proteins 22*, 119−131.
17. Smith, C. K., and Regan, L. (1995) Guidelines for protein design: The energetics of -sheet side chain interactions, *Science 270*, 980−982.
18. Ho, S. N., Hunt, H. D., Horton, R. M., Pullen, J. K., and Pease, L. R. (1989) Site-directed mutagenesis by overlap extension using the polymerase chain reaction, *Gene 77*, 51−59.
19. Berliner, L. J., Grunwald, J., Hankovszky, H. O., and Hideg, K. (1982) A novel reversible thiol-specific spin label: papain active site labeling and inhibition, *Anal. Biochem. 119*, 450−455.
20. Levin, M. S., Locke, B., Yang, N. C., Li, E., and Gordon, J. I. (1988) Comparison of the ligand binding properties of two homologous rat apocellular retinol-binding proteins expressed in *Escherichia coli*, *J. Biol. Chem. 263*, 17715−17723.
21. Gross, A., Columbus, L., Hideg, K., Altenbach, C., and Hubbell, W. L. (1999) Structure of the KcsA potassium channel from *Streptomyces lividans*: a site-directed spin labeling study of the second transmembrane segment, *Biochemistry 38*, 10324−10335.
22. Altenbach, C., Oh, K. J., Trabanino, R. J., Hideg, K., and Hubbell, W. L. (2001) Estimation of inter-residue distances in spin labeled proteins at physiological temperatures: experimental strategies and practical limitations, *Biochemistry 40*, 15471−15482.
23. Hubbell, W. L., Froncisz, W., and Hyde, J. S. (1987) Continuous and stopped flow EPR spectrometer based on a loop gap resonator, *Rev. Sci. Instrum. 58*, 1879−1886.
24. Altenbach, C., Flitsch, S., Khorana, H. G., and Hubbell, W. L. (1989) Structural studies on transmembrane proteins. 2. Spin labeling of bacteriorhodopsin mutants at unique cysteines, *Biochemistry 28*, 7806−7812.
25. Budil, D. E., Lee, S., Saxena, S., and Freed, J. H. (1996) Nonlinear-least-squares analysis of slow-motion EPR spectra in one and two dimensions using a modifies Levenberg−Marquardt algorithm, *J. Magn. Reson., Ser. A 120*, 155−189.
26. Schneider, D. J., and Freed, J. H. (1989) Calculating slow motional magnetic resonance spectra, in *Biological Magnetic Resonance* (Berliner, L. J., Reuben, J., Ed.) pp 1−76, Plenum Publishing Corp., New York.
27. Freed, J. H. (1976) Theory of slow tumbling ESR spectra for nitroxides, in *Spin Labeling: Theory and Applications* (Berliner, L. J., Ed.), pp 53−132, Academic Press, New York.
28. Lovell, S. C., Word, J. M., Richardson, J. S., and Richardson, D. C. (2000) The penultimate rotamer library, *Proteins 40*, 389−408.
29. van Wart, H. E., and Scheraga, H. A. (1977) Stable conformations of aliphatic disulfides: influence of 1,4 interactions involving sulfur atoms, *Proc. Natl. Acad. Sci. U.S.A. 74*, 13−17.
30. Petersen, M. T. N., Jonson, P. H., and Petersen, S. B. (1999) Amino acid neighbours and detailed conformational analysis of cysteines in proteins, *Prot. Eng. 12*, 535−548.
31. Dunbrack, R., Jr., and Karplus, M. (1994) Conformational analysis of the backbone-dependent rotamer preferences of protein sidechains, *Nat. Struct. Biol. 1*, 334−340.
32. Nemethy, G., and Scheraga, H. A. (1981) Strong interaction between disulfide derivatives and aromatic groups in peptides and proteins, *Biochem. Biophys. Res. Commun. 98*, 482−487.

BI0360962